# Off-resonance 13C–2H REDOR NMR for site-resolved studies of molecular motion

# Off-Resonance $^{13}C$-$^{2}H$ REDOR NMR for Site-Resolved Studies of Molecular Motion

Martin D. Gelenter, Kelly J. Chen, and Mei Hong*

Department of Chemistry, Massachusetts Institute of Technology, 77 Massachusetts Avenue, Cambridge, MA 02139

* Corresponding author: Mei Hong: meihong@mit.edu

Revised for ***J. Biomol. NMR***

June 21, 2021

**Abstract**

We introduce a $^{13}C$-$^{2}H$ Rotational Echo DOuble Resonance (REDOR) technique that uses the difference between on-resonance and off-resonance $^{2}H$ irradiation to detect dynamic segments in deuterated molecules. By selectively inverting specific regions of the $^{2}H$ magic-angle spinning (MAS) sideband manifold to recouple some of the deuterons to nearby carbons, we distinguish dynamic and rigid residues in 1D and 2D $^{13}C$ spectra. We demonstrate this approach on deuterated GB1, H/D exchanged GB1, and perdeuterated bacterial cellulose. Numerical simulations reproduce the measured mixing-time and $^{2}H$ carrier-frequency dependence of the REDOR dephasing of bacterial cellulose. Combining numerical simulations with experiments thus allow the extraction of motionally averaged quadrupolar couplings from REDOR dephasing values.

**Keywords:** protein dynamics, cellulose, quadrupolar coupling, deuterium NMR

## Introduction

Molecular motions drive a myriad of biological processes such as enzyme catalysis, ion conduction, substrate transport, and signaling (Hilger et al. 2018; Latorraca et al. 2017; Mandala et al. 2018; Wright and Dyson 2015). Macromolecular dynamics also influence the properties of biomaterials such as cell walls (Dick-Pérez et al. 2011; Wang et al. 2016). While X-ray crystallography and cryo-electron microscopy (cryoEM) are excellent methods for determining the structures of biomacromolecules, they are ineffective for providing information about the rates and amplitudes of molecular motion. In comparison, NMR spectroscopy is well suited to elucidate molecular motions over a wide range of timescales (Lewandowski et al. 2015). Specifically, solid-state NMR spectroscopy is not limited to soluble molecules (Reif et al. 2021) but can be applied to study motions of biological macromolecules in a variety of environments such as lipid bilayers (Mandala et al. 2020), cell walls (Kang et al. 2019) and biofilms (McCrate et al. 2013).

A large number of solid-state NMR techniques have been developed to characterize the amplitudes of molecular motion. Among these, measurements of motionally averaged dipolar couplings (Munowitz et al. 1981) and quadrupolar couplings (Witterbort et al. 1987) are especially advantageous. The uniaxial nature of the dipolar coupling tensor makes it a simple probe of the reorientational geometry (Schmidt-Rohr and Spiess 1994), whereas the large size of quadrupolar couplings makes them sensitive to small reorientational angles. Among quadrupolar nuclei, the spin-1 deuterium has long been exploited for probing molecular motion (Alam et al. 1991; Browning and Seelig 1980; Davis 1983; Gall et al. 1982; Kinsey et al. 1981; Struts et al. 2011; Witterbort et al. 1987) because of the ease of deuterating biomolecules and the favorable magnitude of $^{2}$H quadrupolar couplings in organic compounds. The rigid-limit quadrupolar coupling constant ($C_Q$) of aliphatic deuterons (CD, $CD_2$, $CD_3$) is ~170 kHz, which is six-fold larger than the rigid-limit one-bond $^{1}$H-$^{13}$C dipolar coupling. The OD and ND groups have even larger rigid-limit $C_Q$ values of 200–250 kHz. These quadrupolar couplings are sufficiently large to be sensitive to small motional amplitudes, without being too large to complicate the excitation and inversion of the $^{2}$H NMR spectra. Like $^{1}$H-$^{13}$C dipolar couplings, the $^{2}$H quadrupolar tensor of aliphatic deuterons is uniaxial and aligned with the C-H bond. Due to these favorable properties, static $^{2}$H NMR has been used for many decades to characterize the rates and geometry of motions in biomolecules such as phospholipids (Seelig 1977) and nucleic acids (Meints et al. 2001). However, static $^{2}$H NMR is limited to singly deuterated compounds. To obtain dynamics information about perdeuterated proteins or other biomolecules, magic-angle-spinning (MAS) $^{2}$H NMR experiments are necessary. Recently, 2D and 3D $^{13}$C-$^{2}$H correlation experiments were introduced to correlate $^{2}$H quadrupolar couplings with $^{13}$C chemical shifts (Gelenter et al. 2017; Hologne et al. 2005; Shi and Rienstra 2016). These experiments encode the $^{2}$H qudrupolar couplings in the indirect dimension and resolve the sideband patterns by one or two $^{13}$C chemical shift dimensions. These methods have been demonstrated on model compounds, but their sensitivity is limited due to the low polarization transfer efficiency between $^{2}$H and $^{13}$C and the low sensitivity of $^{2}$H excitation (Jain et al. 2014).

Rotational-echo DOuble Resonance (REDOR) is a widely used and robust approach to recouple heteronuclear dipolar couplings under MAS using two 180˚ pulses in each rotation period (Gullion and Schaefer 1989). REDOR has been applied to a wide range of systems for distance measurements (Cegelski 2013; Reif et al. 2021). For fixed internuclear distances in dynamic molecules, REDOR can be used to measure motionally averaged dipolar couplings to obtain information about motional geometry (Schanda et al. 2010). Here we introduce a $^{13}$C-$^{2}$H REDOR technique (**Fig. 1**) that probes site-specific dynamics by off-resonance and selective dipolar dephasing of molecules with large $^{2}$H quadrupolar couplings. Although $^{13}$C-$^{2}$H REDOR NMR has been explored before for distance measurements in rigid solids (Cady et al. 2010; Sack et al. 2000; Sack et al. 1999), the incomplete inversion of the $^{2}$H spectra with typical rf



2

field strengths of ~50 kHz causes slower and more featureless dipolar dephasing compared to the theoretical dephasing. Here we exploit weak $^{2}$H rf field strengths that are 1.1-1.5 times the MAS frequency to selectively recouple different regions of the $^{2}$H NMR spectra. By applying $^{2}$H 180˚ pulses far off resonance to invert deuterons with large quadrupolar couplings, we cause selective dephasing of immobilized C-D bonds. These off-resonance spectra are then subtracted from near-resonance spectra where both rigid and dynamic groups are recoupled, to yield difference spectra that exhibit the signals of only dynamic moieties. This experimental approach works best at slow to moderate MAS frequencies 10-15 kHz, in order to retain the quadrupolar coupling anisotropy and to allow weak and selective $^{2}$H rf field strengths to be used. We demonstrate this off-resonance $^{13}$C-$^{2}$H REDOR method on $^{13}$C, $^{15}$N, $^{2}$H-labeled GB1 (CDN-GB1), $^{13}$C, $^{15}$N-labeled H/D exchanged GB1, and $^{13}$C, $^{2}$H-labeled bacterial cellulose. We show that this approach readily distinguishes mobile groups from rigid groups, and can be applied in a 2D $^{13}$C-$^{13}$C correlation fashion to measured site-resolved dynamics. We further evaluate the dependence of $^{13}$C-$^{2}$H REDOR dephasing on the $^{2}$H resonance offset using numerical simulations for deuterated bacterial cellulose.

## Materials and Methods

### *Sample Preparation*

The CDN-GB1 sample used in this study was expressed in *E. coli* as previously described (Franks et al. 2005; Gelenter et al. 2017). The protein was purified using size-exclusion chromatography, and the protein solution was concentrated to 30 mg/ml in 70% $D_2O$. To produce microcrystalline protein, 1 ml of the GB1 solution was mixed with three 1 ml aliquots of the crystalizing solution, which contains 2-methyl-2,4-pentanediol (MPD) and isopropanol (IPA) at a 2:1 ratio. The concentrated solution was not properly buffered, leading to crystallization occurring at unoptimal pH. This led to imperfect microcrystals, which give rise to broader linewidths than GB1 crystallized under ideal conditions. $^{13}$C, $^{15}$N-labeled and protonated GB1 was expressed similarly (Franks et al. 2005; Gelenter et al. 2017). For H/D exchange, the protein solution was concentrated to 40 mg/ml using an Amicon Ultra-15 concentrator with a 5 kDa molecular weight cut off (Millipore). This solution was exchanged with $D_2O$ to reach an estimated deuteration level of 96% before being concentrated to 20 mg/ml for crystallization. The deuteration level was estimated to be 80% for labile sites by comparing $^{15}$N CP and DP spectral intensities.

$^{13}$C, $^{2}$H-labeled bacterial cellulose was produced from *Acetobacter xylinus* sub sp. *sucrofermentans* (ATCC 700178) and purified using a previously published procedure (Bali et al. 2013; Gelenter et al. 2017; He et al. 2014). The growth medium contained 98% $D_2O$ with U-$^{13}$C6 and 1,2,3,4,5,6,6-$D_7$ labeled D-glucose as the sole carbon source. After 2 weeks of growth at room temperature, the cellulose pellicles were frozen at -20˚C and ground to a slurry using a Waring blender. The bacterial debris was removed by successive washing in 1% NaOD until the supernatant $A_{280}$ absorbance was < 0.01. Finally, cellulose was neutralized by washing with $D_2O$ until the pH of the surrounding solvent reached ~7.

### *Solid-state NMR experiments and data analysis*

Solid-state NMR experiments were conducted on a 600 MHz (14.1 T) Bruker Avance III HD spectrometer using a 3.2 mm $^{1}$H/$^{13}$C/$^{2}$H MAS probe. $^{13}$C chemical shifts were referenced to the $CH_2$ peak of adamantane at 38.48 ppm on the tetramethylsilane (TMS) scale (Morcombe and Zilm 2003). Experiments on GB1 were conducted under 14 kHz MAS at a set temperature of 268 K, while experiments on bacterial cellulose were conducted under 10 kHz MAS at a set temperature of 278 K. Due to frictional heating, the true sample temperature is 10-15 K higher than the set temperature (Bernard et al. 2017).

Experiments on GB1 began with $^{1}$H-$^{13}$C cross-polarization (CP) (Pines et al. 1972), while experiments on deuterated bacterial cellulose began with $^{2}$H-$^{13}$C Rotor Echo Short Pulse IRradiATION

cross-polarization ($^{RESPIRATION}$CP) (Jain et al. 2012). GB1 samples were spun at 14 kHz MAS, while deuterated bacterial cellulose was spun at 10 kHz MAS. Rectangular $^{13}$C 90° and 180° pulses used an rf field strength of 50 kHz. $^{2}$H 180˚ REDOR pulse field strengths were set to 11.1 kHz for experiments on bacterial cellulose and 20 kHz for experiments on GB1. The $^{13}$C Gaussian 180° pulse during the REDOR period on H/D GB1 was 285 μs ($4\tau_r$) to selectively invert and refocus the $^{13}$Cα and $^{13}$Cβ polarization. For the two GB1 samples, $^{1}$H two-phase pulse-modulation (TPPM) decoupling (Bennett et al. 1995) was applied at a field strength of 71 kHz during both the REDOR period and the $^{13}$C acquisition period. No $^{1}$H decoupling was used for deuterated cellulose, which allowed a short recycle delay of 0.75-1.0 s to be used for these experiments. A recycle delay of 2.0 s was used for both GB1 samples. The $^{13}$C acquisition times were 13.5 ms in all experiments, while the indirect $^{13}$C dimension of the 2D $^{13}$C-$^{13}$C correlation experiments used a maximum evolution time of 4.1 ms.

***Numerical simulations***

The $^{13}$C-$^{2}$H REDOR dephasing was read off as the intensity ratio of the dephased spectrum S and the control spectrum $S_0$ as a function of mixing time. The REDOR dephasing as a function of $^{2}$H rf carrier frequency was simulated using the software SpinEvolution (Veshtort and Griffin 2006). We considered a four-spin system as a simplified model of bacterial cellulose, consisting of the C6 carbon and the three aliphatic deuterons that are the closest to C6: the two C6 deuterons and the C5-bonded deuteron (Nishiyama et al. 2003). All simulations were run with either a quadrupolar coupling constant ($C_Q$) of 170 kHz and an asymmetry parameter η of 0 or a $C_Q$ of 85 kHz and an η of 1. In both cases the Euler angles were set to (0, 0, 0), which aligns the principal axis of the $^{2}$H quadrupolar coupling tensor with the z-axis of the crystallite frame, which is the same orientation as the $^{2}$H-$^{13}$C dipolar coupling. The $^{1}$H Larmor frequency was set to 600 MHz and the chemical shift anisotropy (CSA) was not included for either $^{2}$H or $^{13}$C. Inclusion of the CSA for $^{13}$C did not alter the simulations results. Simulations were run for an MAS frequency of 10 kHz and a rectangular $^{2}$H 180˚ pulse at an rf field strength of 11.1 kHz. The simulation pulse sequence consisted of the $^{RESPIRATION}$CP and REDOR portions of the experimental pulse sequence used for bacterial cellulose (**Fig. 1c**). REDOR dephasing curves were simulated for $^{2}$H carrier frequencies between -250 and 250 kHz in 5 kHz increments. All simulations were carried out using the ^rep2000 set of Euler angles, which uses the REPULSION powder averaging scheme (Bak and Nielsen 1997) and an n_gamma value of 20, where n_gamma specifies powder averaging over the third angle. We found that this choice both avoids irregularities and is computationally faster than other sets of Euler angles, such as the ASG method (Alderman et al. 1986).

**Results**

**Fig. 2** shows the 1D $^{13}$C and $^{2}$H MAS spectra of CDN-GB1, H/D exchanged GB1, and CD-labeled bacteria cellulose. All three samples are hydrated with $D_2O$. The $^{13}$C CP-MAS spectra (**Fig. 2a-c**) show the $^{13}$C chemical shift resolution of these macromolecules, while the $^{2}$H MAS sideband spectra (**Fig. 2d-f**) illustrate the overlap of multiple types of deuterons in deuterated and hydrated samples. First, the deuterated water gives rise to a high isotropic peak that dominates the spinning sidebands of the anisotropic deuterons. Second, in CDN-GB1, the sideband intensities of both rigid aliphatic groups with a $C_Q$ of ~170 kHz and mobile methyl groups with motionally averaged $C_Q$'s overlap. In H/D exchanged GB1, the signals of rigid backbone amide deuterons overlap with the signals of mobile sidechain deuterons such as the lysine amines (**Fig. 2e**). In bacterial cellulose, most deuterons have rigid-limit $C_Q$'s of ~170 kHz (**Fig. 2f**), while a small fraction of deuterons have smaller quadrupolar couplings (Gelenter et al. 2017). However, the latter's contribution to the overlapped 1D $^{2}$H spectrum cannot be easily resolved.

***Off-resonance $^{2}$H REDOR dephasing depends on the quadrupolar coupling strength***



4

**Fig. 3** shows the $^{13}C$ spectra of CDN-GB1 and H/D GB1 under on-resonance ($^{2}H$ carrier frequency at 0 kHz) and +70-kHz off-resonance $^{2}H$ REDOR pulses. The $^{2}H$ rf field strengths were 20 kHz in these experiments. For CDN-GB1 (**Fig. 3a, b**), REDOR dephasing is observed for all $^{13}C$ sites, but the amount of dephasing, as manifested by the difference spectrum (ΔS), differs depending on the $^{13}C$-$^{2}H$ dipolar couplings. Carbonyl carbons show much less dephasing than aliphatic carbons, as expected due to the lack of a directly bonded deuteron. Between on-resonance and off-resonance $^{2}H$ irradiation, on-resonance irradiation caused larger dephasing, with higher ΔS intensities. This can be attributed to the larger fraction of intensities in the center of the $^{2}H$ spectrum. The methyl $^{13}C$ signals show much higher ΔS intensities in the on-resonance REDOR spectrum than the off-resonance spectrum. This is consistent with motional averaging of the methyl $^{2}H$ quadrupolar coupling as well as $^{13}C$-$^{2}H$ dipolar coupling, which make far-off-resonance $^{2}H$ pulses ineffective for inverting the methyl $^{2}H$ coherence. Thus, off-resonance $^{2}H$ REDOR pulses dephase rigid deuterons more than they dephase mobile deuterons.

The $^{13}C$-$^{2}H$ REDOR spectra of H/D exchanged GB1 (**Fig. 3c-e**) selectively detect the $^{13}C$ sites that are in close proximity to labile hydrogens such as backbone amide deuterons and sidechain OD and ND groups. Since these exchanged deuterons are not directly bonded to carbons, the REDOR mixing time required for observing dipolar dephasing is longer than that of CDN-GB1. We found that a mixing time of 7.1 ms was ideal for observing dephasing while retaining sufficient $^{13}C$ spectral intensities. To remove the $^{13}C\alpha$-$^{13}CO$ J-coupling during the mixing time, we applied a selective $^{13}C\alpha$ Gaussian 180° pulse (Jaroniec et al. 1999). The bandwidth of this Gaussian 180° pulse was such that some $^{13}C\beta$ signals with chemical shifts near the $^{13}C\alpha$ region were also refocused. The on-resonance and off-resonance $^{2}H$-dephased REDOR difference spectra are similar for this sample, with the off-resonance spectrum giving slightly lower difference intensities compared to the on-resonance $^{2}H$-dephased spectrum due to the lower $^{2}H$ spectral intensity at an offset of +70 kHz compared to the on-resonance case.

***2D $^{13}C$-$^{13}C$ resolved $^{13}C$-$^{2}H$ REDOR spectra of GB1***

To obtain site-resolved information for $^{13}C$-$^{2}H$ REDOR dephasing, we conducted a 2D $^{13}C$-$^{13}C$ resolved $^{13}C$-$^{2}H$ REDOR experiment using a 30 ms $^{13}C$ CORD mixing period (Hou et al. 2013) (**Fig. 1a**). The 2D spectra show the $^{2}H$-dephased $^{13}C$ signals in the indirect dimension while the direct dimension provides site resolution. We first demonstrate this experiment on CDN-GB1 (**Fig. 4**), and compare the difference spectrum (ΔS) measured under on-resonance and +70-kHz off-resonance $^{2}H$ irradiation. The $^{2}H$ rf field strengths were 20 kHz in these experiments. When on-resonance $^{2}H$ pulses were applied for 1.7 ms, difference intensities are observed for both methyl carbons between 15 and 22 ppm (**Fig. 4b**) and for other aliphatic carbons between 70 and 40 ppm. When +70 kHz off-resonance $^{2}H$ REDOR pulses were applied, we obtained a distinct ΔS spectrum in which the methyl carbons exhibit minimal dephasing while Cα and Cβ carbons show similar dipolar dephasing as the on-resonance ΔS spectrum (**Fig. 4c**). Taking the difference between the two ΔS spectra yielded a ΔΔS spectrum that only exhibits the signals of mobile deuterons (**Fig. 4d**). Most of these ΔΔS signals can be assigned to methyl carbons of Val, Thr, and Ala residues and carbons in dynamic Lys sidechains. We note that some peaks are overlapped in the 2D $^{13}C$-$^{13}C$ spectra, and we only annotate those peaks that can be site-specifically assigned to a single residue. In addition, some dynamic loop residues such as G41, E42, and E56 are also observed in the ΔΔS spectrum. The G41 and E56 difference peaks appear in the carbonyl region of the 2D spectrum, which is not shown here. **Fig. 4e** shows the GB1 structure (PDB code: 2LGI (Wylie et al. 2011)) in which sites that are detected in the ΔΔS spectrum are indicated as orange sticks.

Application of the off-resonance $^{13}C$-$^{2}H$ REDOR experiment to H/D exchanged GB1 yielded a different ΔΔS spectral pattern (**Fig. 5**). Since only solvent-exposed labile deuterons such as backbone amide deuteron and sidechain hydroxyl and amide deuterons are present in this sample, the difference



5

between the on-resonance (**Fig. 5b**) and +70 kHz off-resonance REDOR spectra (**Fig. 5c**) reveal those exchangeable deuterons that are dynamic. **Fig 5d** shows that the most dynamic exchangeable deuterons result from the Cε of lysine sidechains such as K13 and K28 and Cα sites of residues such as M1, Q2, D47, A48 and E56. These residues are located in the loops of the protein, whose amide groups are more mobile than those of most other residues (**Fig. 5e**). In addition, some of the helical residues such as A24, E27, Q32 and N35, which face the protein exterior, also exhibit significant conformational dynamics. We attribute this observation to loose crystal packing that renders these residues flexible, while residues facing the protein interior are immobilized by sidechain interactions and backbone hydrogen bonding.

***Dependence of off-resonance $^{13}C$-$^{2}H$ REDOR on the $^{2}H$ carrier frequency: bacterial cellulose***

To further evaluate off-resonance $^{13}C$-$^{2}H$ REDOR dephasing, we compared the experimental spectra of $^{13}C$, $^{2}H$-labeled bacterial cellulose (**Fig. 6a, b**) with simulated REDOR dephasing (Veshtort and Griffin 2006). Deuterated bacterial cellulose is a good model system for analyzing $^{13}C$-$^{2}H$ REDOR because of its highly resolved 1D $^{13}C$ spectrum (**Fig. 6c**) and the known quadrupolar couplings for its deuterons (Gelenter et al. 2017). Five out of the six glucose CD groups have rigid-limit $^{2}H$ quadrupolar couplings of 170 kHz and an asymmetry parameters of 0. The exception is the deuterons attached to C6 in surface cellulose, which undergo *trans-gauche* isomerization and thus have a quadrupolar coupling of 85 kHz and an asymmetry parameter of 1 (Gelenter et al. 2017). The $^{13}C$ difference spectra measured with $^{2}H$ carrier frequencies of 0, +60 kHz and +120 kHz and a REDOR dephasing period of 1 ms show that the iC6 difference intensity is relatively insensitive to the $^{2}H$ frequency change from 0 to +60 kHz, with $\Delta S/S_0$ values of 0.82 and 0.78, respectively, but the difference intensity decreased to 0.32 when the $^{2}H$ frequency increased to +120 kHz (**Fig. 6c**). While this attenuated dipolar dephasing at the larger $^{2}H$ frequency offset is expected, surface cellulose C6 shows a much larger intensity change with the $^{2}H$ carrier frequency. The sC6 difference intensity decreased by nearly a factor of two (from 0.61 to 0.34) from a $^{2}H$ carrier frequency of 0 to +60 kHz, while at +120 kHz, negligible difference intensity ($\Delta S/S_0$ value of ~0.12) was observed. The narrower $^{2}H$ spinning sideband pattern for the dynamic deuterons bonded to sC6 makes the REDOR dephasing of sC6 more sensitive to changes in the $^{2}H$ carrier offset. Therefore, the dynamic difference between interior and surface C6 hydroxymethyl groups affect the REDOR results.

We measured 1D $^{13}C$-detected REDOR spectra as a function of REDOR mixing times as well as $^{2}H$ resonance offset (**Fig. 6c**). The $^{2}H$ carrier frequency was varied from 0 to +200 kHz in 20 kHz increments, and the REDOR mixing time was varied from 0 to 2 ms in 0.2 ms increments, yielding a total of 121 1D $^{13}C$ spectra. **Fig. 7a, c, d** show the measured and simulated $^{13}C$-$^{2}H$ REDOR dephasing for the rigid interior cellulose C6 peak at 65 ppm, while **Fig. 7b, e, f** show the data for the 61-ppm surface cellulose C6 and simulations using a motionally averaged $^{2}H$ quadrupolar coupling of 85 kHz for the deuterons bonded to C6. The uncertainties in the experimental data are propagated from the measured $S_0$ and S spectra. In both experiments and simulations, the rigid iC6 and the mobile sC6 show similar dipolar dephasing when $^{2}H$ pulses are on resonance. But off-resonance $^{2}H$ irradiation caused larger dipolar dephasing to the rigid iC6 than to the mobile sC6. Larger $^{2}H$ offsets produce less dipolar dephasing compared to small offsets (**Fig. 7a,b**). In both simulation and experiments, there is little dephasing when the $^{2}H$ resonance offset exceeds 120 kHz for rigid CD groups and exceeds 60 kHz for mobile CD groups (**Fig. 7a, b**). Thus rigid and dynamic CD groups can be distinguished based on their REDOR dephasing at $^{2}H$ offsets between 60 and 120 kHz. Simulations show that smaller $^{2}H$ resonance offsets lead to overestimates of dipolar dephasing while larger offsets underestimate dipolar dephasing compared to experiments (**Fig. 7d, f**).

**Discussion**



6

This off-resonance $^{13}C$-$^{2}H$ REDOR method represents a simple and efficient approach for identifying mobile sites in deuterated biomolecules. While direct encoding of a $^{2}H$ dimension and its correlation with $^{13}C$ in 2D or 3D experiments have been demonstrated (Gelenter et al. 2017; Hologne et al. 2005; Shi and Rienstra 2016) and give information about motional order parameters, this correlation approach suffers from low sensitivity because of the low efficiency of $^{2}H$-$^{13}C$ polarization transfer (Jain et al. 2012; Jain et al. 2014; Nielsen et al. 2013) and the explicit encoding of a $^{2}H$ dimension. $^{2}H$-$^{13}C$ correlation experiments also do not easily benefit from cross polarization from $^{1}H$ spins. In perdeuterated biomolecules, the sparseness of protons necessitates the use of $^{2}H$ as the excitation nucleus. Although fast relaxation of $^{2}H$ spins in principle allows the use of short recycle delays (Borle and Seelig 1983), in practice the recycle delays cannot be too short in order to avoid high rf duty cycles. For partially protonated biomolecules, $^{1}H$ decoupling is required, thus long recycle delays are still necessary (McNeill et al. 2009). The current off-resonance $^{13}C$-$^{2}H$ REDOR approach overcomes these limitations by using traditional $^{1}H$-$^{13}C$ CP to create the initial $^{13}C$ magnetization, by obviating a $^{2}H$ dimension, and by avoiding $^{2}H$ polarization transfer to $^{13}C$. Instead, we encode the dynamics information as different extents of dipolar dephasing between on-resonance and off-resonance $^{2}H$ pulses. Mobile carbons show strong dephasing with on-resonance $^{2}H$ REDOR pulses but attenuated dephasing when the $^{2}H$ pulses are far off-resonance. In this way, the $\Delta\Delta S$ spectra exhibit the signals of dynamic groups. Although the 2D $^{13}C$-$^{13}C$ resolved off-resonance $^{13}C$-$^{2}H$ REDOR experiment gives only qualitative information about the mobile residues, it is possible to make this method more quantitative by choosing several $^{2}H$ resonance offsets and mixing times, and simulating the resulting dephasing as shown for bacterial cellulose (**Fig. 7**). The current off-resonance $^{13}C$-$^{2}H$ REDOR approach works best under moderate MAS frequencies where the anisotropic $^{2}H$ quadupolar interaction is retained in each rotation period and where weak $^{2}H$ 180˚ pulses can be applied to selectively invert the deuterons at a given frequency offset. Numerical simulations for MAS frequencies of 10-40 kHz and $^{2}H$ rf field strengths from 11.1 to 66.7 kHz (**Fig. 8**) confirm this expectation. Using the surface cellulose C6 quadrupolar coupling parameters as an example, we find that increasing the $^{2}H$ rf field strength broadened the frequency range that exhibit significant REDOR dephasing and slowed down the dephasing at 10 kHz MAS. Increasing the MAS frequency to 20 kHz decreased the offset dependence of REDOR dephasing due to better averaging of the quadrupolar couplings. REDOR oscillations occur at larger offsets, which would complicate the extraction of the mobile sites. Increasing the MAS frequency to 40 kHz further decreased the offset dependence of REDOR dephasing.

Compared to the 2D $^{13}C$-$^{13}C$ resolved $^{13}C$-$^{1}H$ DIPSHIFT method (Dregni et al. 2019) for quantifying the amplitude of motion, the off-resonance $^{13}C$-$^{2}H$ REDOR method differs by indirectly probing the motional averaging of the $^{2}H$ quadrupolar spectra. Because the $^{2}H$ quadupolar coupling of a CD group is 6-fold larger than the one-bond $^{13}C$-$^{1}H$ dipolar coupling, $^{2}H$ quadrupolar coupling is a more accurate reporter of dynamics. Moreover, labile hydrogens such as NH and OH are at least two bonds away from a $^{13}C$ spin, thus they are not easily amenable to the $^{13}C$-$^{1}H$ DIPSHIFT experiment. In comparison, NH and OH groups can be analyzed through $^{2}H$ NMR spectra. Therefore, off-resonance $^{13}C$-$^{2}H$ REDOR is a sensitive probe of the dynamics of residues that contain labile hydrogens.

In conclusion, we have demonstrated an off-resonance $^{13}C$-$^{2}H$ REDOR technique for investigating the dynamics of perdeuterated or H/D exchanged biomolecules. This approach uses the difference between on-resonance and off-resonance $^{2}H$ irradiated $^{13}C$-$^{2}H$ REDOR spectra to identify mobile residues. This method is simple to use, and has similar sensitivity and resolution as regular 2D $^{13}C$-$^{13}C$ correlation spectra. We envision this technique to be especially useful for characterizing the motion of segments containing exchangeable protons, where no easy alternative methods are available for detecting motion.

**Data Availability Statement**



7

1D and 2D spectral datasets and Bruker pulse programs are available upon request from Mei Hong at meihong@mit.edu.

**Acknowledgements**

This work is supported by NIH grant AG059661 to M.H. The bacterial cellulose work is supported by the Center for Lignocellulose Structure and Formation, an Energy Frontier Research Center funded by the U.S. Department of Energy, Office of Science, Basic Energy Sciences under Award # DE-SC0001090. M.D.G. is supported by an NIH Ruth L. Kirschstein Individual National Research Service Award (1F31AI133989).

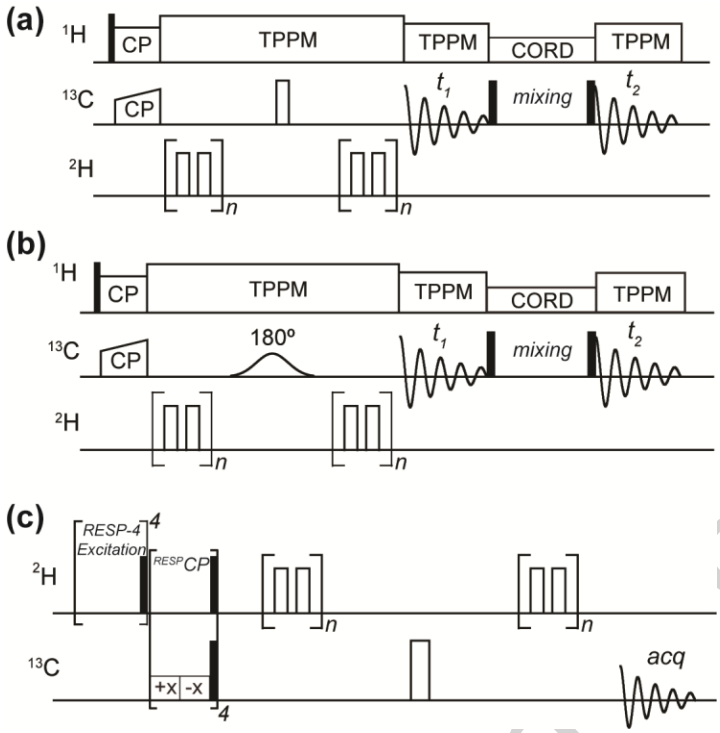


**Figure 1.** Pulse sequences for off-resonance $^{13}C$-$^{2}H$ REDOR experiments. (**a**) Broadband 2D $^{13}C$-$^{13}C$ correlation with $^{13}C$-$^{2}H$ REDOR dephasing. (**b**) Cα/Cβ-selective 2D $^{13}C$-$^{13}C$ correlation with $^{13}C$-$^{2}H$ REDOR dephasing. The 1D variants of the pulse sequences in (**a**) and (**b**) acquire the signals during the $t_1$ period and omit the pulses after that step. (**c**) 1D $^{13}C$-$^{2}H$ REDOR with $^{2}H$-$^{13}C$ $^{respiration}$CP to generate the initial $^{13}C$ magnetization. This experiment was applied to perdeuterated bacterial cellulose.





9

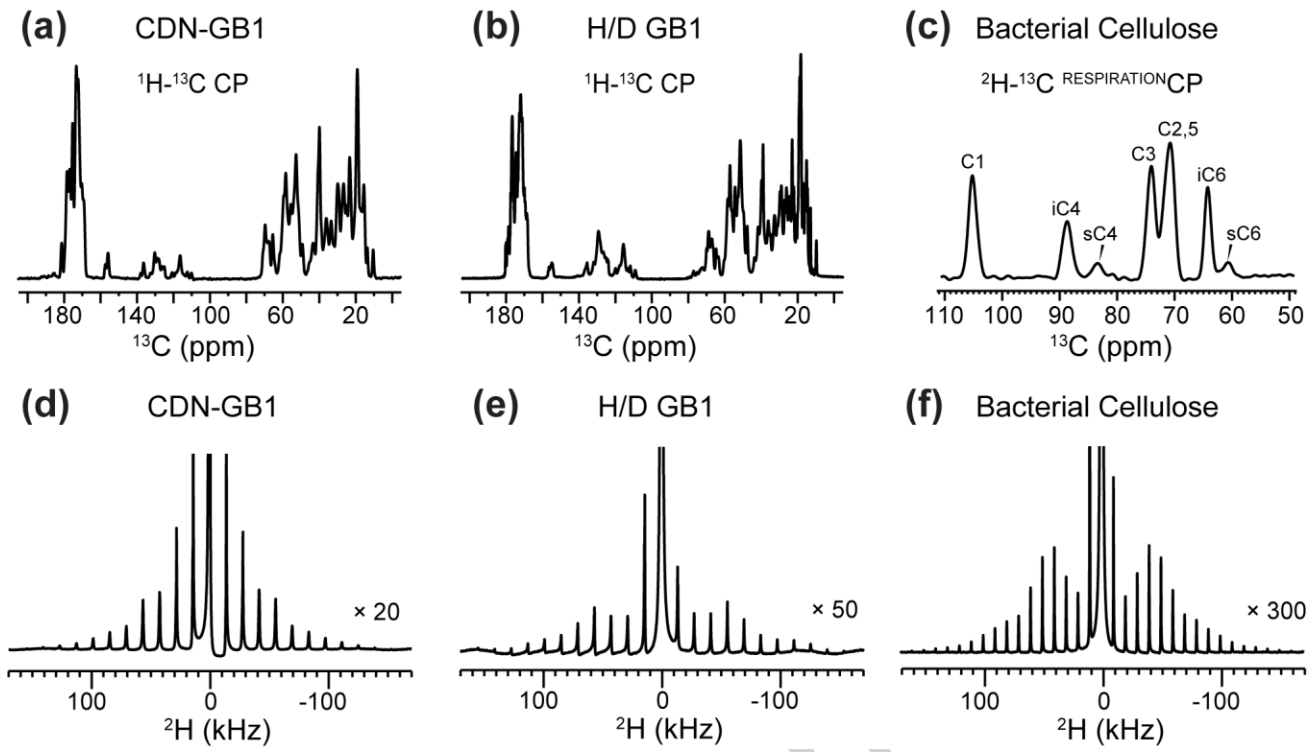


**Figure 2**. 1D $^{13}$C (**a-c**) and $^{2}$H (**d-f**) MAS spectra of GB1 and bacterial cellulose. (**a, d**) CDN-GB1. (**b, e**) H/D exchanged $^{13}$C, $^{15}$N-labeled GB1. (**c, f**) Perdeuterated bacterial cellulose. All $^{2}$H MAS spectra were measured using RESPIRATION-4 excitation. The CDN-GB1 and H/D-GB1 spectra were measured under 14 kHz MAS while the bacterial cellulse spectra were measured under 10 kHz MAS.

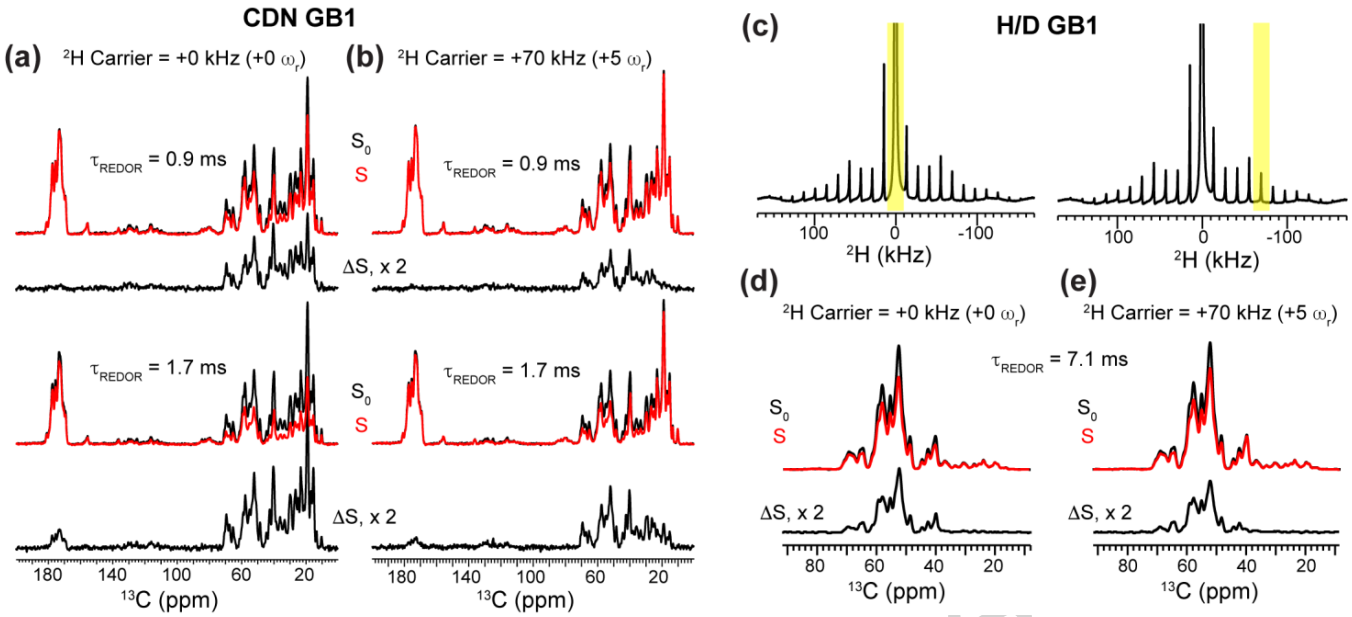


**Figure 3**. $^{13}C$-$^{2}H$ REDOR spectra of CDN-GB1 and H/D exchanged GB1. (**a**) $^{13}C$ REDOR spectra of CDN-GB1 with on-resonance $^{2}H$ REDOR pulses. The $^{2}H$ rf field strength is 20 kHz. The control $S_0$, dephased S, and difference ΔS spectra are shown. (**b**) $^{13}C$ REDOR spectra of CDN-GB1 with 70 kHz off-resonance $^{2}H$ REDOR pulses. Little dephasing is observed for the sidechain methyl peaks. (**c**) $^{2}H$ MAS spectra of H/D exchanged GB1. The centerband and the +70-kHz sideband peaks are highlighted in yellow. (**d**) $^{13}C$ REDOR spectra of H/D exchanged GB1 with on-resonance $^{2}H$ REDOR pulses. (**e**) $^{13}C$ REDOR spectra of H/D exchanged GB1 with 70 kHz off-resonance $^{2}H$ REDOR pulses. All spectra were measured under 14 kHz MAS on the 600 MHz spectrometer.





11

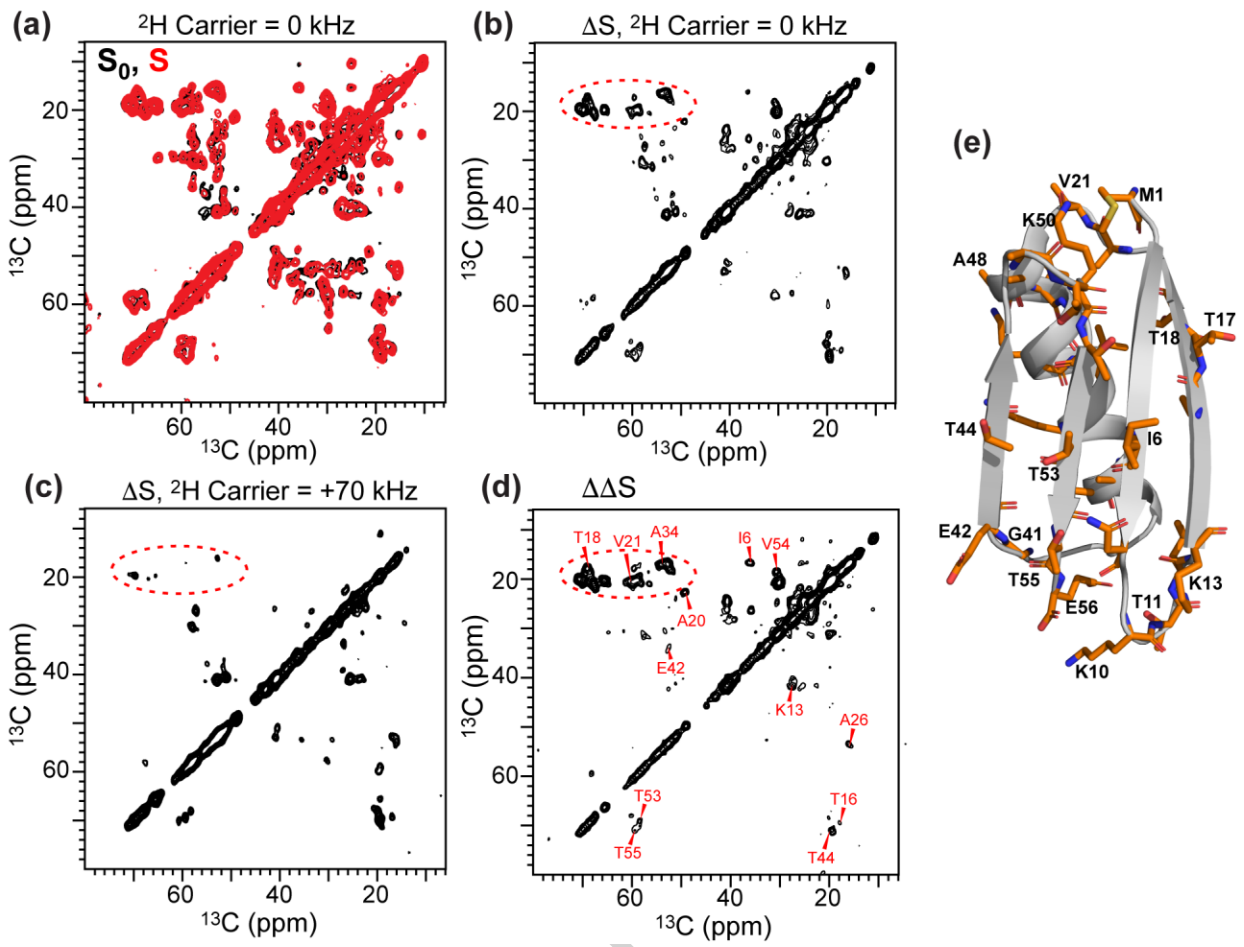


**Figure 4**. 2D $^{13}C$-$^{13}C$ resolved $^{13}C$- $^{2}H$ REDOR spectra of CDN-GB1. The spectra were measured under 14 kHz MAS using a REDOR mixing time of 1.7 ms, and $^{2}H$ and $^{13}C$ REDOR rf field strengths of 20 kHz and 50 kHz, respectively. (**a**) $S_0$ (black) and S (red) 2D spectra with on-resonance $^{2}H$ REDOR pulses. Most $^{13}C$ signals show similar extents of dipolar dephasing. (**b**) ΔS spectrum obtained from the on-resonance $^{2}H$ REDOR pulses. (**c**) ΔS spectrum when the $^{2}H$ REDOR pulses are 70 kHz off resonance. Little dephasing is observed for the methyl peaks. (**d**) ΔΔS spectrum between the on- and off-resonance ΔS spectra. The observed peaks result from dynamic residues. (**e**) Dynamic residues whose $^{13}C$ signals are detected in the ΔΔS spectrum are shown as orange sticks.





12

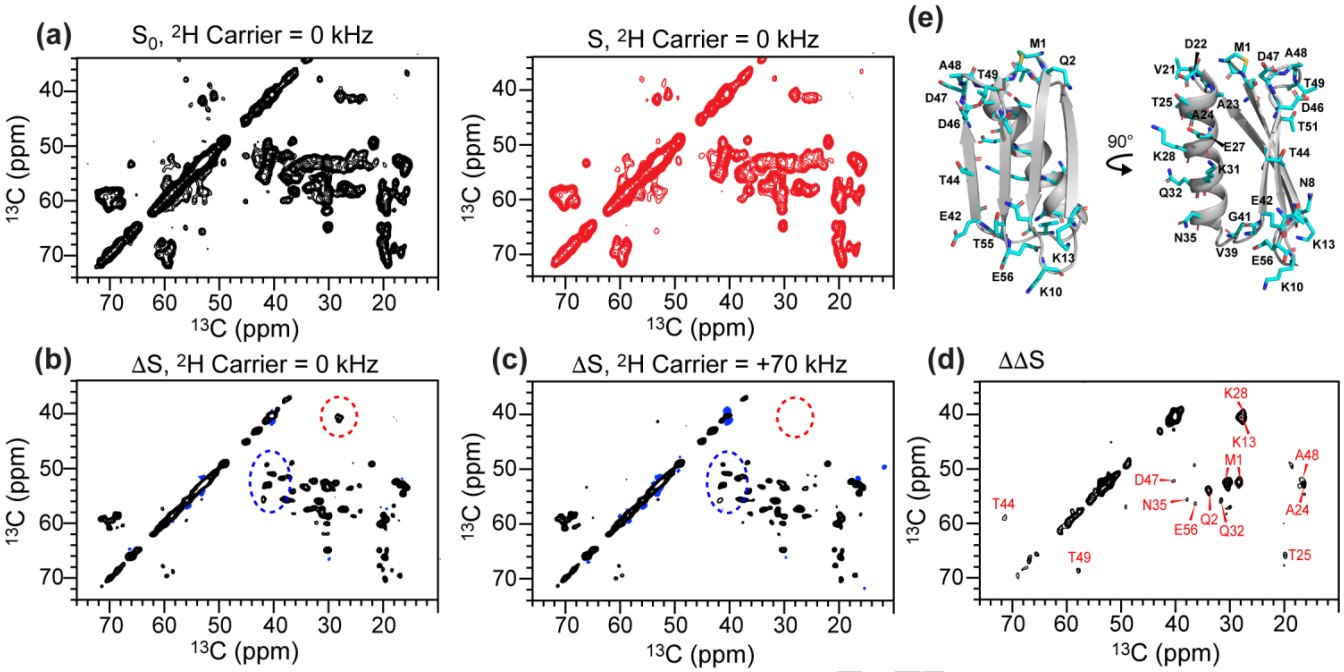


**Figure 5.** 2D $^{13}C$-$^{13}C$ resolved $^{13}C$-$^{2}H$ REDOR spectra of H/D GB1. The spectra were measured with a REDOR mixing time of 7.1 ms under 14 kHz MAS. The rf field strengths of REDOR pulses were 20 kHz for $^{2}H$ and 50 kHz for $^{13}C$. (**a**) $S_0$ (black) and S (red) 2D spectra measured with on-resonance $^{2}H$ REDOR dephasing pulses. (**b**) ΔS spectrum obtained from the on-resonance $S_0$ and S spectra in (**a**). (**c**) ΔS spectrum for 70 kHz off-resonance $^{2}H$ REDOR pulses. Note that some methyl carbons (red dashed circle) are better dephased in the on-resonance ΔS spectrum than the off-resonance ΔS spectrum. Blue dashed circle highlight carbons that are similarly dephased in the on-resonance and off-resonance REDOR spectra. (**d**) ΔΔS spectrum between the on-resonance and off-resonance ΔS spectra. These $^{13}C$ signals result from dynamic residues containing exhchangeable hydrogens. (**e**) Dynamic residues identified in the ΔΔS spectrum.





13

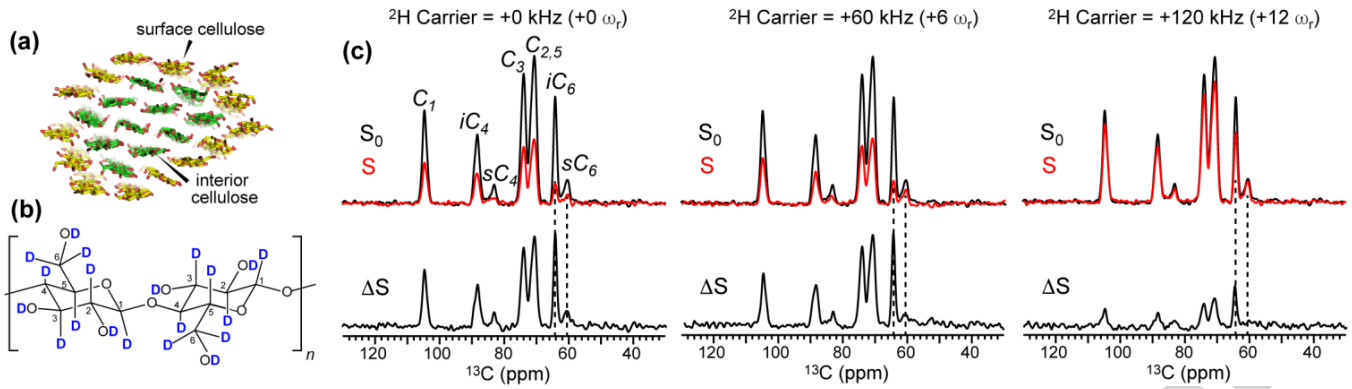


**Figure 6.** $^{13}C$-$^{2}H$ REDOR data of perdeuterated bacterial cellulose. (**a**) Bacterial cellulose fibrils showing interior cellulose in green and surface cellulose in yellow. (**b**) Chemical structure of cellulose. C6 is the only carbon not on the sugar backbone. (**c**) 1D $^{13}C$ detected and $^{2}H$-dephased REDOR $S_0$, S and ΔS spectra with 1.0 ms REDOR mixing. The spectra were measured with $^{2}H$ REDOR on resonance, 60 kHz off resonance, and 120 kHz off resonance, under 10 kHz MAS.





14

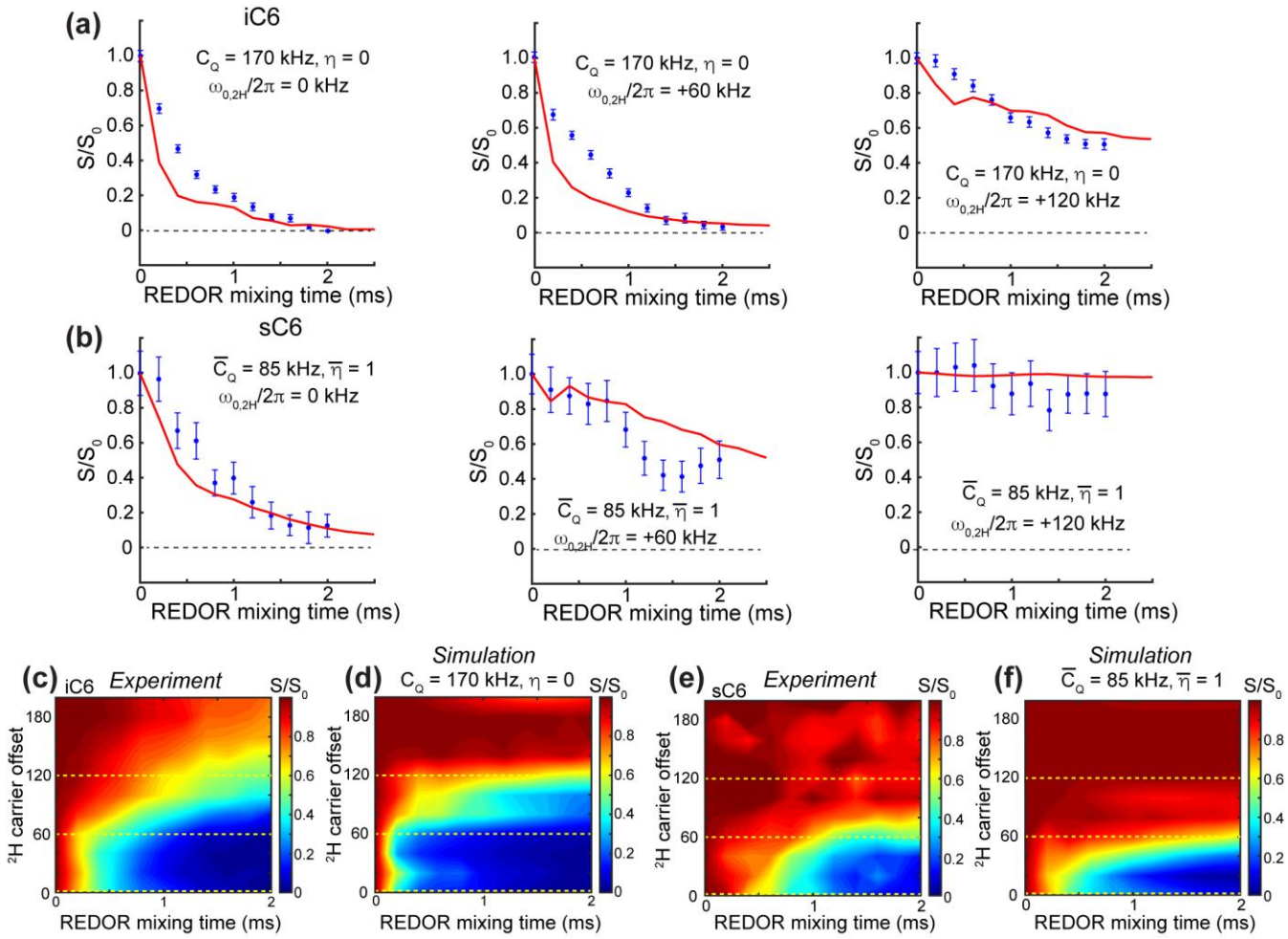


**Figure 7**. Numerical simulations of $^{13}C$-$^{2}H$ REDOR dephasing for 10 kHz MAS compared to experimentally measured dephasing for bacterial cellulose. (**a**) $^{13}C$-$^{2}H$ REDOR dephasing curves for interior C6, with $^{2}H$ resonance offsets of 0, +60 and +120 kHz, and simulations using a four spin system in which all three $^{2}H$ nuclei have a $C_Q$ of 170 kHz and η = 0. (**b**) $^{13}C$-$^{2}H$ REDOR dephasing curves for surface C6, with $^{2}H$ resonance offsets of 0, +60 and +120 kHz, and simulations using a four spin system in which the two $^{2}H$ nuclei bonded to C6 have a motionally averaged $C_Q$ of 85 kHz and a motionally averaged η of 1, while the $^{2}H$ nucleus bonded to C5 has a rigid limit $C_Q$ of 170 kHz and η = 0. (**c**) Measured $^{13}C$-$^{2}H$ REDOR dephasing map for interior C6 as a function of REDOR mixing time and $^{2}H$ resonance offset. (**d**) Simulated 2D $^{13}C$-$^{2}H$ REDOR dephasing maps for interior C6 sites; all three deuterons in this simulation have a rigid-limit $C_Q$ of 170 kHz and η = 0. (**e**) Measured $^{13}C$-$^{2}H$ REDOR dephasing maps for surface C6 deuterons as a function of REDOR mixing time and $^{2}H$ resonance offset. (**f**) Simulated 2D $^{13}C$-$^{2}H$ REDOR dephasing maps for surface C6 sites, including a motionally averaged quadrupolar coupling of 85 kHz and a motionally averaged η of 1 for the deuterons bonded to C6.





15

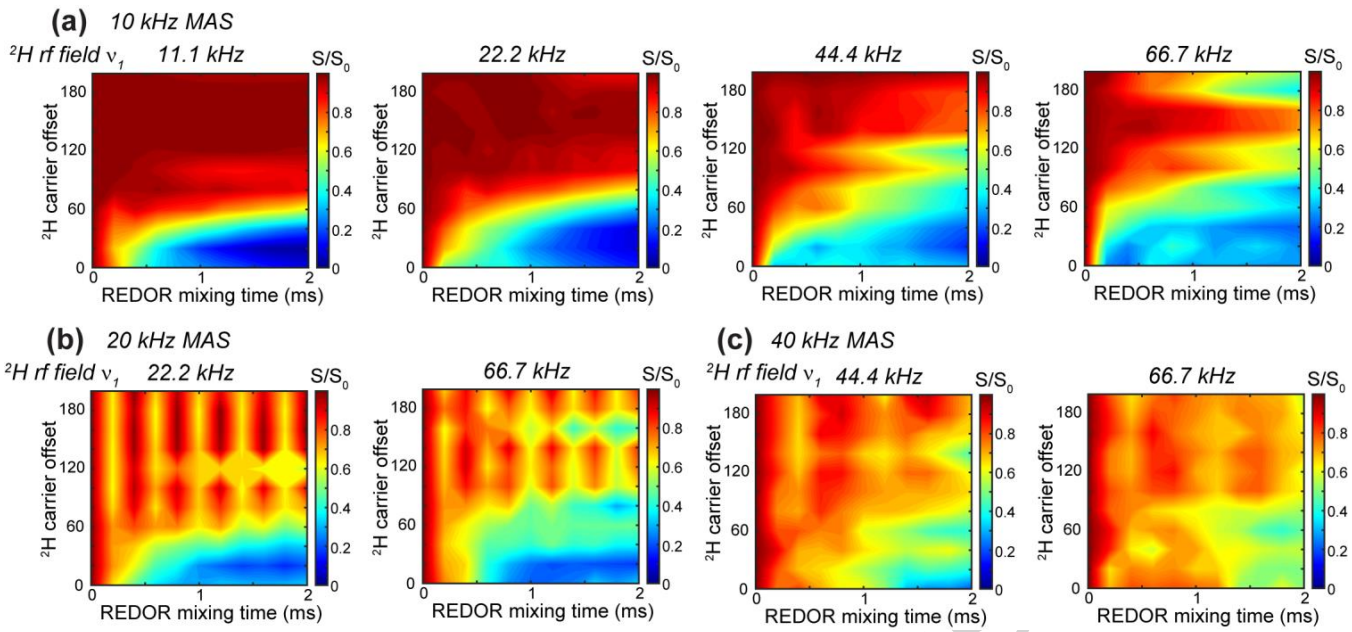


**Figure 8**. Numerical simulations of the dependence of $^{13}C$-$^{2}H$ REDOR dephasing on MAS frequency and $^{2}H$ rf field strength ($\nu_1$). Simulations used the quadrupolar coupling parameters of surface C6 deuterons in bacterial cellulose, with a motionally averaged quadrupolar coupling of 85 kHz and a motionally averaged η of 1. (**a**) Simulated REDOR dephasing for 10 kHz MAS with $^{2}H$ rf field strengths of 11.1 kHz to 66.7 kHz. These conditions correspond to 90% to 15% of each rotation period being occupied by the two $^{2}H$ 180˚ pulses. The weaker the $^{2}H$ rf field strengths, the more selective the REDOR dephasing, with low $S/S_0$ values. (**b**) Simulated REDOR dephasing for 20 kHz MAS with $^{2}H$ rf field strengths of 22.2 kHz and 66.7 kHz. These conditions correspond to 90% and 30% of each rotation period being occupied by the $^{2}H$ pulses. (**c**) Simulated REDOR dephasing for 40 kHz MAS with $^{2}H$ rf field strengths of 44.4 kHz and 66.7 kHz, which correspond to 90% and 60% of each rotation period being occupied by the $^{2}H$ pulses. REDOR dephasing becomes less frequency-selective with increasing MAS frequencies.





16

**References**

Alam TM, Orban J, Drobny GP (1991) Deuterium NMR investigation of backbone dynamics in the synthetic oligonucleotide [d(CGCGAATTCGCG)]2 Biochemistry 30:9229-9237

Alderman DW, Solum MS, Grant DM (1986) Methods for analyzing spectroscopic line shapes. NMR solid powder patterns J Chem Phys 84:3717-3725

Bak M, Nielsen NC (1997) REPULSION, A Novel Approach to Efficient Powder Averaging in Solid-State NMR J Magn Reson 125:132-139

Bali G, Foston MB, O'Neill HM, Evans BR, He J, Ragauskas AJ (2013) The effect of deuteration on the structure of bacterial cellulose Carbohyd Res 374:82-88

Bennett AE, Rienstra CM, Auger M, Lakshmi KV, Griffin RG (1995) Heteronuclear decoupling in rotating solids J Chem Phys 103:6951-6958

Bernard GM, Goyal A, Miskolzie M, McKay R, Wu Q, Wasylishen RE, Michaelis VK (2017) Methylammonium lead chloride: A sensitive sample for an accurate NMR thermometer J Magn Reson 283:14-21

Borle F, Seelig J (1983) Hydration of Escherichia coli lipids: Deuterium T1 relaxation time studies of phosphatidylglycerol, phosphatidylethanolamine and phosphatidylcholine Biochim Biophys Acta, Biomembr 735:131-136

Browning JL, Seelig J (1980) Bilayers of phosphatidylserine: a deuterium and phosphorus nuclear magnetic resonance study. Biochemistry 19:1262-1270

Cady SD, Schmidt-Rohr K, Wang J, Soto CS, DeGrado WF, Hong M (2010) Structure of the amantadine binding site of influenza M2 proton channels in lipid bilayers Nature 463:689-692

Cegelski L (2013) REDOR NMR for drug discovery Bioorg Med Chem Lett 23:5767-5775

Davis JH (1983) The description of membrane lipid conformation, order and dynamics by 2H-NMR. Biochim Biophys Acta 737:117-171

Dick-Pérez M, Zhang Y, Hayes J, Salazar A, Zabotina OA, Hong M (2011) Structure and Interactions of Plant Cell-Wall Polysaccharides by Two- and Three-Dimensional Magic-Angle-Spinning Solid-State NMR Biochemistry-US 50:989-1000

Dregni AJ et al. (2019) In vitro 0N4R tau fibrils contain a monomorphic β-sheet core enclosed by dynamically heterogeneous fuzzy coat segments Proc Natl Acad Sci U S A 116:16357-16366

Franks WT et al. (2005) Magic-Angle Spinning Solid-State NMR Spectroscopy of the β1 Immunoglobulin Binding Domain of Protein G (GB1): $^{15}$N and $^{13}$C Chemical Shift Assignments and Conformational Analysis J Am Chem Soc 127:12291-12305

Gall CM, Cross TA, DiVerdi JA, Opella SJ (1982) Protein dynamics by solid-state NMR: aromatic rings of the coat protein in fd bacteriophage Proc Natl Acad Sci U S A 79:101-105



17

Gelenter MD, Wang T, Liao SY, O'Neill H, Hong M (2017) (2)H-(13)C correlation solid-state NMR for investigating dynamics and water accessibilities of proteins and carbohydrates J Biomol NMR 68:257-270

Gullion T, Schaefer J (1989) Rotational-echo double-resonance NMR J Magn Reson 81:196-200

He J et al. (2014) Controlled incorporation of deuterium into bacterial cellulose Cellulose 21:927-936

Hilger D, Masureel M, Kobilka BK (2018) Structure and dynamics of GPCR signaling complexes Nat Struct Mol Biol 25:4-12

Hologne M, Faelber K, Diehl A, Reif B (2005) Characterization of dynamics of perdeuterated proteins by MAS solid-state NMR J Am Chem Soc 127:11208-11209

Hou G, Yan S, Trébosc J, Amoureux JP, Polenova T (2013) Broadband homonuclear correlation spectroscopy driven by combined R2(n)(v) sequences under fast magic angle spinning for NMR structural analysis of organic and biological solids J Magn Reson 232:18-30

Jain S, Bjerring M, Nielsen NC (2012) Efficient and Robust Heteronuclear Cross-Polarization for High-Speed-Spinning Biological Solid-State NMR Spectroscopy J Phys Chem Lett 3:703-708

Jain SK et al. (2014) Low-power polarization transfer between deuterons and spin-1/2 nuclei using adiabatic (RESPIRATION)CP in solid-state NMR Phys Chem Chem Phys 16:2827-2830

Jaroniec CP, Tounge BA, Rienstra CM, Herzfeld J, Griffin RG (1999) Measurement of 13C−15N Distances in Uniformly 13C Labeled Biomolecules: J-Decoupled REDOR J Am Chem Soc 121:10237-10238

Kang X, Kirui A, Dickwella Widanage MC, Mentink-Vigier F, Cosgrove DJ, Wang T (2019) Lignin-polysaccharide interactions in plant secondary cell walls revealed by solid-state NMR Nat Commun 10:347

Kinsey RA, Kintanar A, Tsai MD, Smith RL, Janes N, Oldfield E (1981) First observation of amino acid side chain dynamics in membrane proteins using high field deuterium nuclear magnetic resonance spectroscopy J Biol Chem 256:4146-4149

Latorraca NR, Venkatakrishnan AJ, Dror RO (2017) GPCR Dynamics: Structures in Motion Chem Rev 117:139-155

Lewandowski JR, Halse ME, Blackledge M, Emsley L (2015) Protein dynamics. Direct observation of hierarchical protein dynamics Science 348:578-581

Mandala VS, McKay MJ, Shcherbakov AA, Dregni AJ, Kolocouris A, Hong M (2020) Structure and drug binding of the SARS-CoV-2 envelope protein transmembrane domain in lipid bilayers Nat Struct Mol Biol 27:1202-1208

Mandala VS, Williams JK, Hong M (2018) Structure and Dynamics of Membrane Proteins from Solid-State NMR Annu Rev Biophys 47:201-222



18

McCrate OA, Zhou X, Reichhardt C, Cegelski L (2013) Sum of the parts: composition and architecture of the bacterial extracellular matrix J Mol Biol 425:4286-4294

McNeill SA, Gor'kov PL, Shetty K, Brey WW, Long JR (2009) A low-E magic angle spinning probe for biological solid state NMR at 750 MHz J Magn Reson 197:135-144

Meints GA, Karlsson T, Drobny GP (2001) Modeling furanose ring dynamics in DNA J Am Chem Soc 123:10030-10038

Morcombe CR, Zilm KW (2003) Chemical shift referencing in MAS solid state NMR J Magn Reson 162:479-486

Munowitz M, Griffin R, Bodenhausen G, Huang T (1981) Two-dimensional rotational spin-echo nuclear magnetic resonance in solids: correlation of chemical shift and dipolar interactions J Am Chem Soc 103:2529-2533

Nielsen AB, Jain S, Ernst M, Meier BH, Nielsen NC (2013) Adiabatic Rotor-Echo-Short-Pulse-Irradiation mediated cross-polarization J Magn Reson 237:147-151

Nishiyama Y, Sugiyama J, Chanzy H, Langan P (2003) Crystal Structure and Hydrogen Bonding System in Cellulose Iα from Synchrotron X-ray and Neutron Fiber Diffraction J Am Chem Soc 125:14300-14306

Pines A, Gibby MG, Waugh JS (1972) Proton-Enhanced Nuclear Induction Spectroscopy. A Method for High Resolution NMR of Dilute Spins in Solids J Chem Phys 56:1776-1777

Reif B, Ashbrook SE, Emsley L, Hong M (2021) Solid-state NMR spectroscopy Nat Rev Methods Primers 1:2

Sack I, Balazs YS, Rahimipour S, Vega S (2000) Solid-state NMR determination of peptide torsion angles: application of 2H-dephased REDOR J Am Chem Soc 122:12263-12269

Sack I, Goldbourt A, Vega S, Buntkowsky G (1999) Deuterium REDOR: Principles and Applications for Distance Measurements J Magn Reson 138:54-65

Schanda P, Meier BH, Ernst M (2010) Quantitative analysis of protein backbone dynamics in microcrystalline ubiquitin by solid-state NMR spectroscopy J Am Chem Soc 132:15957-15967

Schmidt-Rohr K, Spiess HW (1994) Multidimensional Solid-State NMR and Polymers. 1st Ed. edn. Academic Press, San Diego

Seelig J (1977) Deuterium magnetic resonance: theory and application to lipid membranes Q Rev Biophys 10:353-418

Shi X, Rienstra CM (2016) Site-Specific Internal Motions in GB1 Protein Microcrystals Revealed by 3D $^{2}H$–$^{13}C$–$^{13}C$ Solid-State NMR Spectroscopy J Am Chem Soc 138:4105-4119

Struts AV, Salgado GF, Brown MF (2011) Solid-state 2H NMR relaxation illuminates functional dynamics of retinal cofactor in membrane activation of rhodopsin Proc Natl Acad Sci U S A 108:8263-8268



19

Veshtort M, Griffin RG (2006) SPINEVOLUTION: a powerful tool for the simulation of solid and liquid state NMR experiments J Magn Reson 178:248-282

Wang T, Phyo P, Hong M (2016) Multidimensional solid-state NMR spectroscopy of plant cell walls Solid State Nucl Mag 78:56-63

Witterbort RJ, Olejniczak ET, Griffin RG (1987) Analysis of 2H NMR lineshapes in anisotropic media J Chem Phys 86:5411-5420

Wright PE, Dyson HJ (2015) Intrinsically disordered proteins in cellular signalling and regulation Nat Rev Mol Cell Biol 16:18-29

Wylie BJ, Sperling LJ, Nieuwkoop AJ, Franks WT, Oldfield E, Rienstra CM (2011) Ultrahigh resolution protein structures using NMR chemical shift tensors Proc Natl Acad Sci U S A 108:16974-16979

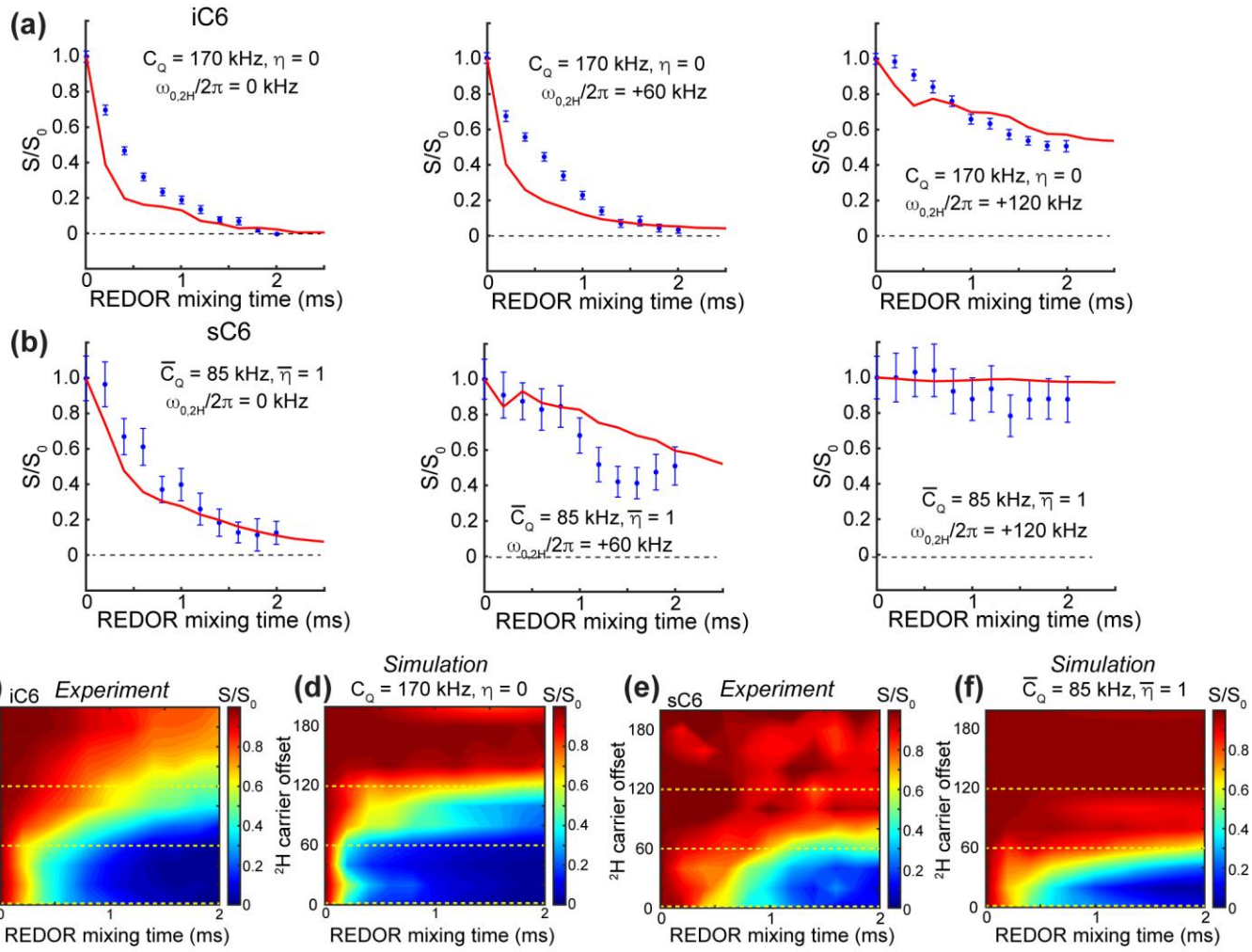
(a)
iC6
$C_Q$ = 170 kHz, η = 0
$\omega_{0,2H}/2\pi$ = 0 kHz
$C_Q$ = 170 kHz, η = 0
$\omega_{0,2H}/2\pi$ = +60 kHz
$C_Q$ = 170 kHz, η = 0
$\omega_{0,2H}/2\pi$ = +120 kHz
(b)
sC6
$\overline{C}_Q$ = 85 kHz, $\overline{\eta}$ = 1
$\omega_{0,2H}/2\pi$ = 0 kHz
$\overline{C}_Q$ = 85 kHz, $\overline{\eta}$ = 1
$\omega_{0,2H}/2\pi$ = +60 kHz
$\overline{C}_Q$ = 85 kHz, $\overline{\eta}$ = 1
$\omega_{0,2H}/2\pi$ = +120 kHz
S/S0
REDOR mixing time (ms)
(c) iC6 Experiment
(d) Simulation
$C_Q$ = 170 kHz, η = 0
(e) sC6 Experiment
(f) Simulation
$\overline{C}_Q$ = 85 kHz, $\overline{\eta}$ = 1
²H carrier offset

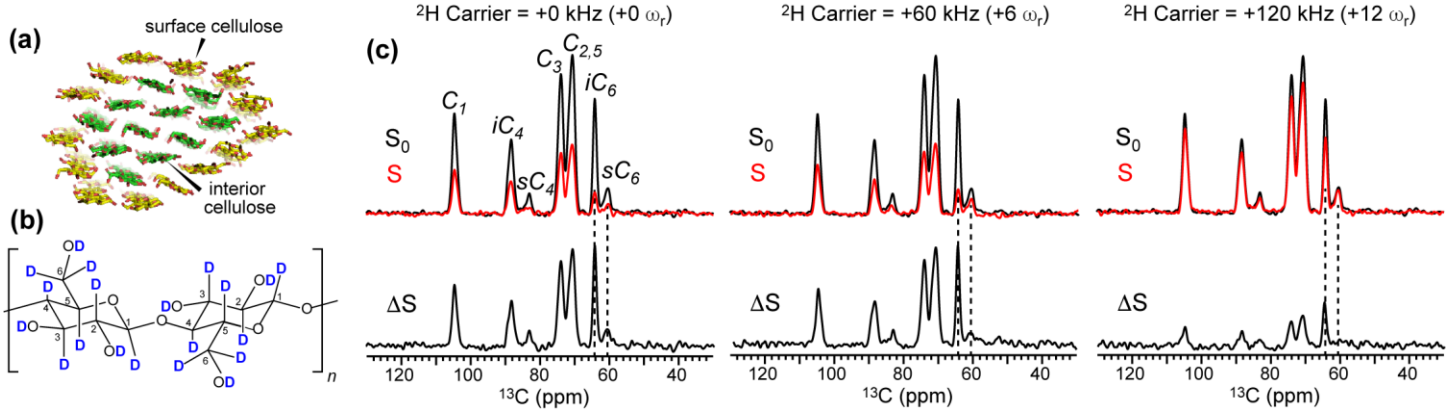
(a)
surface cellulose
interior cellulose
(b)
(c)
²H Carrier = +0 kHz (+0 $\omega_r$)
²H Carrier = +60 kHz (+6 $\omega_r$)
²H Carrier = +120 kHz (+12 $\omega_r$)
$C_1$
$iC_4$
$sC_4$
$C_3$
$C_{2,5}$
$iC_6$
$sC_6$
S0
S
ΔS
¹³C (ppm)



21

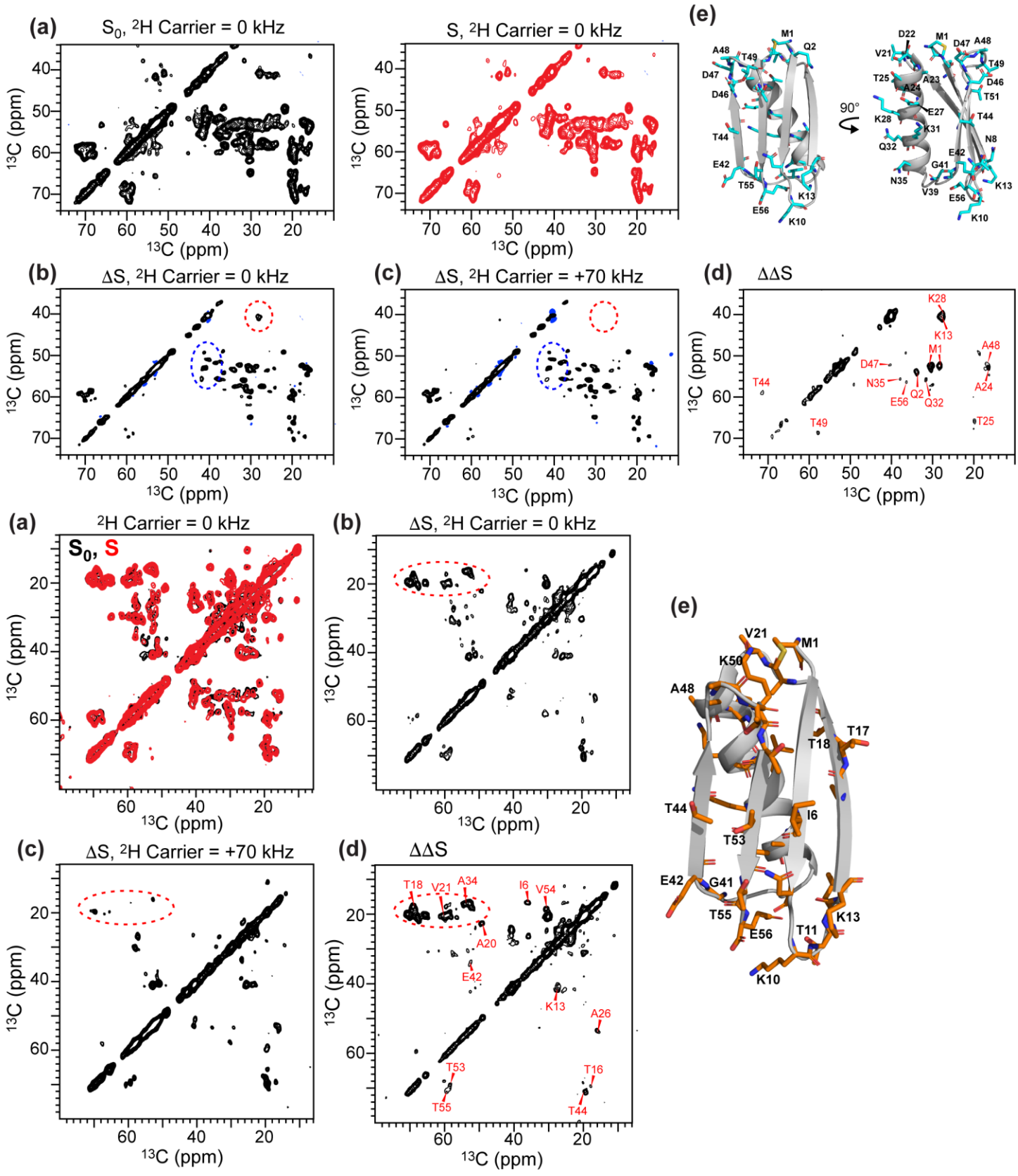
(a)
S0, 2H Carrier = 0 kHz
S, 2H Carrier = 0 kHz
(b)
ΔS, 2H Carrier = 0 kHz
(c)
ΔS, 2H Carrier = +70 kHz
(d)
ΔΔS
(e)
90°
13C (ppm)
(a)
2H Carrier = 0 kHz
S0, S
(b)
ΔS, 2H Carrier = 0 kHz
(c)
ΔS, 2H Carrier = +70 kHz
(d)
ΔΔS
(e)



22

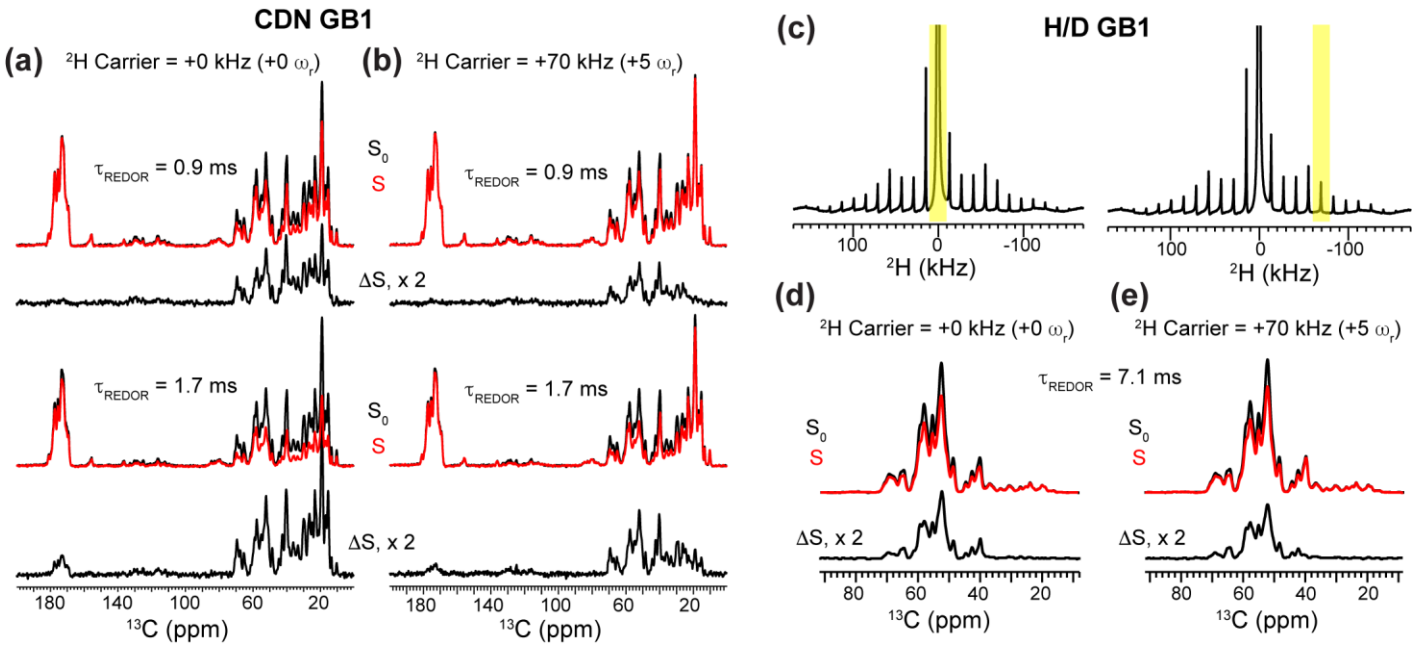
CDN GB1
(a) ²H Carrier = +0 kHz (+0 ω_r)
(b) ²H Carrier = +70 kHz (+5 ω_r)
τ_REDOR = 0.9 ms
τ_REDOR = 1.7 ms
S_0
S
ΔS, x 2
180 140 100 60 20
¹³C (ppm)
(c) H/D GB1
100 0 -100
²H (kHz)
(d) ²H Carrier = +0 kHz (+0 ω_r)
(e) ²H Carrier = +70 kHz (+5 ω_r)
τ_REDOR = 7.1 ms
80 60 40 20

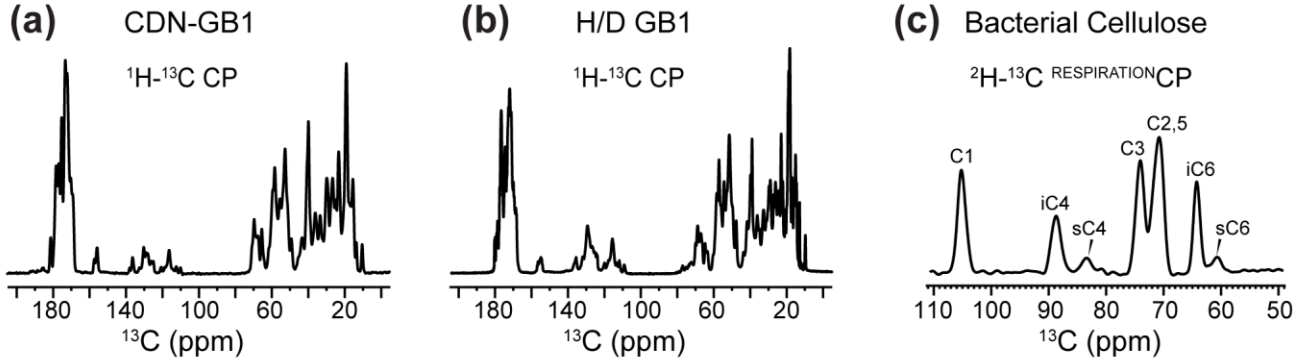
(a) CDN-GB1
¹H-¹³C CP
(b) H/D GB1
¹H-¹³C CP
(c) Bacterial Cellulose
²H-¹³C RESPIRATION CP
C1
iC4
sC4
C3
C2,5
iC6
sC6
180 140 100 60 20
110 100 90 80 70 60 50
¹³C (ppm)

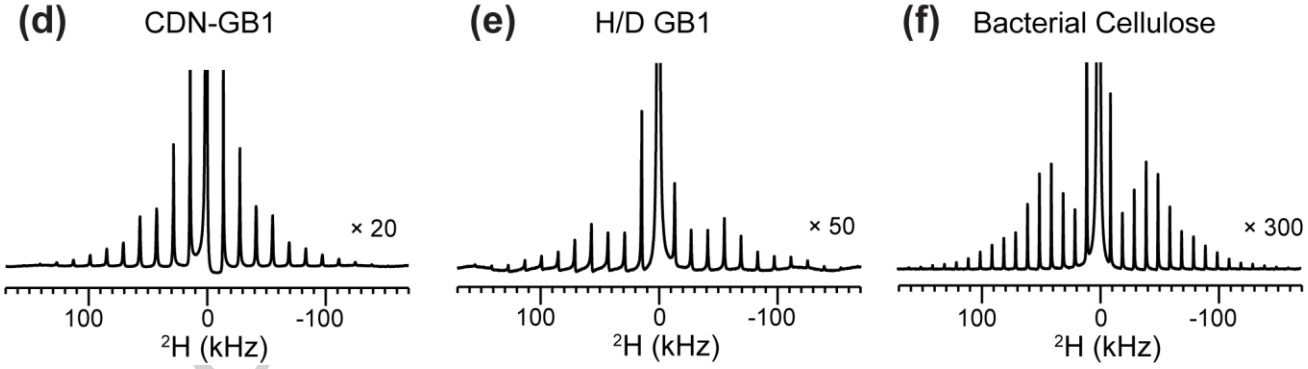
(d) CDN-GB1
(e) H/D GB1
(f) Bacterial Cellulose
× 20
× 50
× 300
100 0 -100
²H (kHz)



23

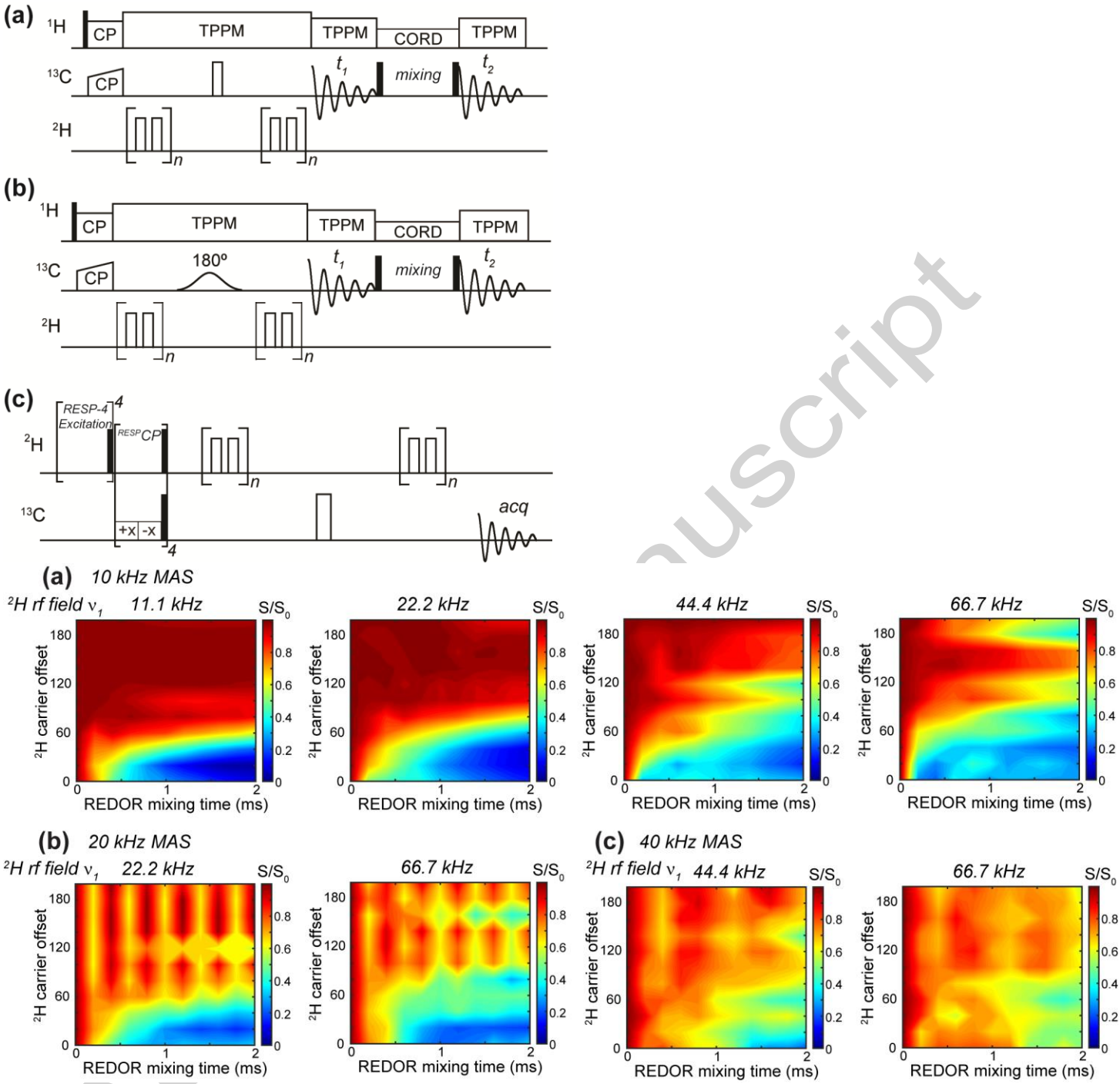
(a)
$^1$H
CP
TPPM
TPPM
CORD
TPPM
$^{13}$C
CP
$t_1$
mixing
$t_2$
$^2$H
n
n
(b)
$^1$H
CP
TPPM
TPPM
CORD
TPPM
$^{13}$C
CP
180°
$t_1$
mixing
$t_2$
$^2$H
n
n
(c)
RESP-4 Excitation
4
$^2$H
RESP CP
n
n
$^{13}$C
+x -x
4
acq
(a) 10 kHz MAS
$^2$H rf field $\nu_1$ 11.1 kHz
22.2 kHz
44.4 kHz
66.7 kHz
S/S$_0$
$^2$H carrier offset
REDOR mixing time (ms)
(b) 20 kHz MAS
$^2$H rf field $\nu_1$ 22.2 kHz
66.7 kHz
(c) 40 kHz MAS
$^2$H rf field $\nu_1$ 44.4 kHz
66.7 kHz



24